Paper presented at the 22nd Asian Conference on Remote Sensing, 5 - 9 November 2001, Singapore.

EXTRACTING BATHYMETRY FROM MULTI-TEMPORAL SPOT IMAGES

Christian MELSHEIMER, LIEW Soo Chin
Centre for Remote Imaging, Sensing and Processing,
Faculty of Science, National University of Singapore,
Blk SOC-1, Lower Kent Ridge Road, Singapore 119260
Tel: (+65) 8746587, Fax: (+65) 7757717
E-mail: crscm@nus.edu.sg
SINGAPORE

KEY WORDS: SPOT, Bathymetry, Radiance, Attenuation

ABSTRACT: In this paper, we investigate the potential of multiple images acquired by the optical/near infrared sensor of the SPOT (Satellite Pour l'Observation de la Terre) satellites for the retrieval of water depth (bathymetry) information. We make use of known methods of depth retrieval from optical data that are based on the attenuation of sunlight by the water column, but in addition we use the known water level differences in multiple images acquired at different stages of the tidal cycle. The known water level difference is used to get an estimate of the attenuation coefficient of the water without having ground truth. The results are reasonable for shallow water.

1. INTRODUCTION

Satellite images acquired by optical sensors, e.g. the High Resolution Visible scanners, HRV, aboard the SPOT (Satellite Pour l'Observation de la Terre) satellites, often show coastal waters in a range of different hues, with darker hues for deeper water and brighter ones for shallow water (see, e.g., Figure 1). This strongly suggests that the images contain information about the water depth (bathymetry). The underlying physical principle is the penetration of sunlight into the water, its reflection by the bottom and its scattering and attenuation by the water column. There are several well-known approaches to retrieve the water depth from optical (mainly Landsat) images, (Benny and Dawson, 1983; Jupp, 1988; Lyzenga, 1978; Philpot, 1989; Green et al., 2000); all of them use the assumed exponential attenuation of light in water; furthermore they use the assumption that the attenuation coefficient is spatially homogeneous.

Whereas usually just one image of a certain area has been used, we try to extend the approach by using multi-temporal images, i.e., multiple images of the same area, which in this case is in the Straits of Malacca. Because of the tide there is a known water-level difference between the different images which can be used to get a rough estimate of the attenuation coefficient and of the water depth near the shore line. In contrast to the single-image approach, we do not use ground truth data.

Knowledge of the bathymetry of coastal waters is of vital importance for ship traffic; remote sensing methods could be at least a cost-effective complement to traditional in-situ sounding methods.

2. BASIC PRINCIPLES: RADIANCE, REFLECTANCE AND ATTENUATION

The radiance L_S measured by the sensor over water of depth z can be written as (Philpot, 1989):

$$L_S(z) = \underbrace{CE_d(0-)(A_B - \rho_\infty)}_{L_S(0)-L_S(\infty)} \exp(-gz) + \underbrace{CE_d(0-)\rho_\infty + L_{SG} + L_{PATH}}_{L_S(\infty)} \quad (1)$$

where C is a transmission factor for atmosphere and water surface; $E_d(0-)$ is the downwelling irradiance just below the water surface; A_B the irradiance reflectance of the bottom (=albedo), assumed to be constant in the area of interest; ρ_∞ is the irradiance reflectance of optically deep water; g the two-way effective attenuation coefficient, assumed to be constant in area of interest; L_{SG} the sun and sky glitter (light reflected to the sensor by the water surface); and L_{PATH} is the path radiance (light scattered to the sensor by the atmosphere). The two-way effective attenuation coefficient g is proportional to the diffuse attenuation coefficient K_d (Mobley, 1994, chap. 3.2), $g = fK_d$, where f is 2 if the sun is in zenith and the sensor is nadir-viewing. For different geometries, f increases as the light path in water becomes longer; details can be found in the appendix A.1. All parameters in the above equation (1) are wavelength dependent, in particular the attenuation coefficient: Over the visible/near-infrared (NIR) range, i.e. from about 400 nm to about 800 nm, K_d and thus g increases by one order of magnitude (Smith and Baker, 1981). We further assume that all parameters are spatially homogeneous.

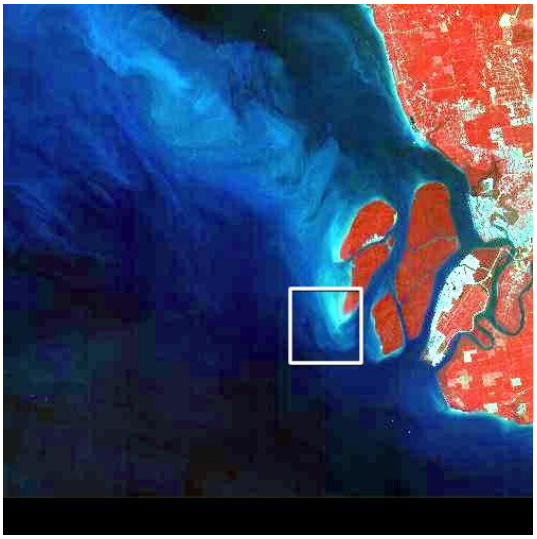

Figure 1: SPOT multispectral image, 22 Jan 1998, 03:40:42 UTC, near Port Klang, West Malaysia, one of the images of the selected area that was used in this study. The white box marks the area that is analyzed in detail. © CNES 1998

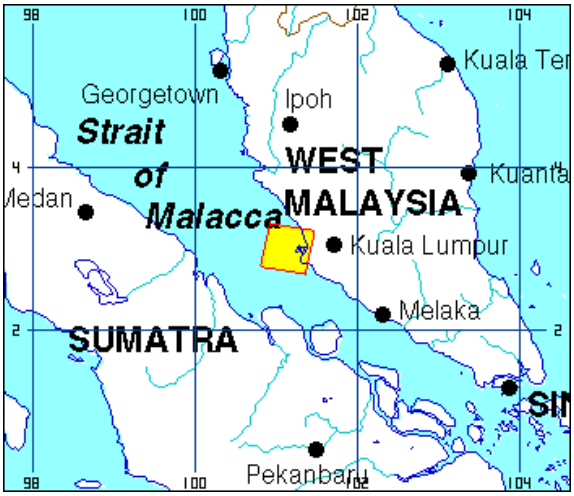

Figure 2: Map showing the location of the test area.

In order to work with a dimensionless quantity, it is common to convert the measured radiance into the so-called top-of-atmosphere reflectance or apparent reflectance R. This is done by dividing the measured radiance L_S by the irradiance received from the sun at the top of the atmosphere and taking account of the solar elevation:

$$R = \frac{\pi L_S}{\cos\zeta F} \tag{2}$$

Here, F is the seasonally varying solar flux and ζ is the zenith angle of the sun. Using this and rearranging the terms of equation (1) as indicated by the underbraces, we get:

$$R(z) = [R(0) - R(\infty)]\exp(-gz) + R(\infty) \tag{3}$$

So if the apparent reflectance for deep water and for zero depth and the attenuation coefficient are known, the last equation can be inverted to get:

$$z = -\frac{1}{g}\left(\log\left[R(z) - R(\infty)\right] - \log\left[R(0) - R(\infty)\right]\right) \tag{4}$$

Whereas the apparent reflectance of deep water and at zero depth can in principle be determined from a remote sensing image, the attenuation coefficient cannot easily be retrieved from from a multispectral remote sensing image. Either hyperspectral data or ground truth – measurements of the attenuation coefficient or point measurements of the depth – are needed. An alternative is to use multiple scenes of the same area, provided there is a known water level difference.

3. MULTIPLE SPOT SCENES

For the present study, we have used multiple SPOT multispectral images of an area near Port Klang on the West coast of West Malaysia, on the shores of the Straits of Malacca (see Figure 2). The area was selected because it has a high tidal amplitude and includes extensive shallow and intertidal areas as well as deep water areas. Being located in the equatorial tropics, the area is usually quite cloudy, and only a few reasonably cloudfree images are available per year. Furthermore, only images with negligible sun glitter (reflection of sunlight by the water surface) were suitable; this was assessed from the imaging geometry (see also Melsheimer and Kwoh, 2001).

We investigated a total of 7 images or "scenes" and focussed mainly on an 8 by 8 km test area that is indicated by a white box in Figure 1. Each scene has three spectral bands: 500-590 nm (band 1, roughly: green visible light),

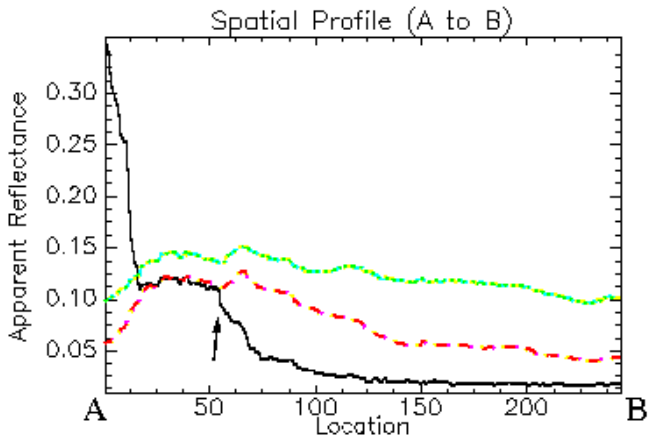

Figure 3: A spatial profile extracted from a multispectral SPOT scene of the test area (22 Jan 1998, 03:40:42 UTC))along the scan line A-B indicated in the image on the right; band 1 (green): green, dashed-dotted; band 2 (red): red, dashed; band 3 (NIR): black, solid. The location of the waterline is marked by an arrow.

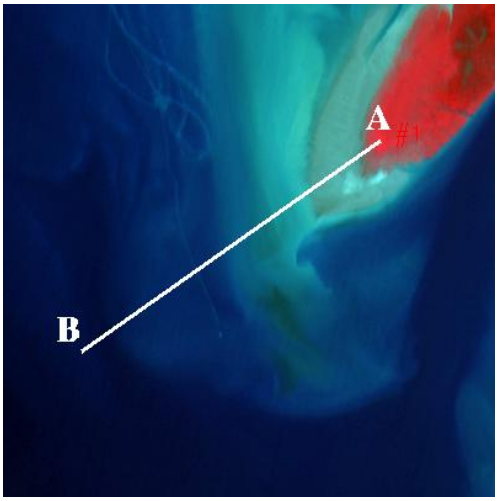

Figure 4: Part of SPOT multispectral image (22 Jan 1998, 03:40:42 UTC), indicating the scan line A-B along which the profile on the left was taken.

610-680 nm (band 2, roughly: red visible light), and 790-890 nm (band 3, near infrared, NIR). The spatial resolution is 20 m. Band 1 (green) has the smallest attenuation coefficient, hence the greatest penetration depth of light, of the order of 10 m, and therefore contains the most information on the bathymetry. In contrast, band 3 (NIR) has a penetration depth of less than 1 m. This fact can be used to determine the water line. Band 2 (red) has not yet been exploited in this study but can be incorporated to improve the results as outlined later (section 5.).

The water level difference between different scenes was determined using tide gauge data and tide tables (Hydrographic Branch, R.M.N., 1997, 1998, 2000). All SPOT scenes were calibrated using the calibration factors provided with the data, and were then converted to apparent reflectance according to equation (2).

4. DATA ANALYSIS

4.1 Determining the Water Line

Knowing the water line in one scene means knowing the water depth along this line in another scene with a higher water level: the depth along that line will be just the water level difference between the two scenes. If a SPOT multispectral scene is displayed as color image, the detectability of the water line is sensitive to the contrast stretching and color balance for the display and is subjective and not reliable. However, we have obtained a more objective method by examining the actual apparent reflectance values along spatial profiles running form vegetation-covered land over exposed tidal flats (sand and mud) toward shallow and deep water. Figure 3 shows one of these profiles. There are two notable features: (1) Vegetation has very high NIR reflectance which makes it easy to mask out areas covered by vegetation just by looking for pixels with the apparent reflectance in band 3 (NIR) higher than in band 1 (green). (2) There is a sharp decline of the NIR apparent reflectance when moving from the exposed tidal flats towards the sea. This decline is consistently found in all analyzed scenes and the only explanation is that it is the water line: The diffuse attenuation coefficient K_d for clear sea water at NIR is about 2 m^{-1} (Smith and Baker, 1981), which means that depth increase of 20 cm reduces the apparent reflectance to 45%. This means that the water line is where the NIR value in the profile starts to decrease (moving from land towards sea). Only in case the water is extremely shallow and the slope of the bottom is extremely small, i.e., only a few decimeters within several hundred meters, the transition is less clear. This is the case in the upper left part of the image. In addition, we found that the NIR apparent reflectance value where the decrease at the water line starts is consistent throughout a scene. Thus, we can read off a threshold or rather a narrow range of NIR values that corresponds to the waterline.

4.2 Estimating the Attenuation Coefficient

We now try to estimate the attenuation coefficient using the water line information and a ratio of the same band in two scenes. Starting from equation (3), if we subtract the deep water value, we get a pure exponential term on the right

hand side:

$$X(z) \equiv R(z) - R(\infty) = [R(0) - R(\infty)] \exp(-gz) \tag{5}$$

Now we take the natural logarithm of the ratio of this quantity for two scenes "a" and "b" with a water level difference d. Scene "a" has the lower water level and we therefore it call the "reference scene".

$$Y_{a,b} \equiv \log(X_a/X_b) = \log \frac{R_a(0) - R_a(\infty)}{R_b(0) - R_b(\infty)} + \Delta g z + g_b d \tag{6}$$

where z is the depth in scene "a", the subscripts denote the scenes "a" and "b", and $\Delta g = g_a - g_b$. The first term on the right-hand side ultimately contains the bottom albedo and the atmospheric conditions (see equation (1)). If we assume that the bottom albedo has not changed and that the atmospheric conditions are similar, this term is negligible. The second term is linear in depth and contains the difference of the attenuation coefficients, and the third term finally is the product of d (which is known) and g_b. Using the method described in the previous section (4.1), we can determine pixels along the water line of scene "a", i.e., pixels where $z = 0$. For these pixels, the second term in the above equation (6) vanished as well. By averaging the log ratio $Y_{a,b}$ over those pixels, we get an estimate of $g_b d$ and hence an estimate of the effective two-way attenuation coefficient for scene "b", g_b.

We applied the analysis just described to band 1 (green) of various pairs of scenes, and we found that indeed the log ratio has its minimum near the water line and increases with depth. There is a considerable amount of noise; however, histograms of the log ratio $Y_{a,b}$ for all the water line pixels of the respective scene "a" were unimodal and reasonably peaked.

4.3 Determining the Depth

With the estimate of the attenuation coefficient, equation (4) can be used to calculate the depth. Using band 1 (green), we determined the deep water value of the apparent reflectance $R(\infty)$ from a suitable area of deep water (depth $>$ 20 m). For the value at zero depth, $R(0)$, using the water line as determined above is not appropriate: The apparent reflectance of exposed tidal flats was found to be variable and often considerably lower than the apparent reflectance of the the shallowest water. So to make sure not to include pixels of the edge of the tidal flats, we had to use pixels slightly seaward from the water line. A resulting depth map, derived from two scenes, is shown in Figure 5, after smoothing with a moving 3×3 average and overlaying with colors and contour lines. The reference scene ("a") was acquired on 27 March, 1998, 03:38:52 UTC, at a water level of 1.2 m; the other scene ("b") from which the depth was calculated was acquired on 22 January, 1998, 03:40:42 UTC, at a water level of 3.9 m.

5. DISCUSSION OF RESULTS

The depth map in Figure 5 shows reasonable depth in the shallow areas. Note that it was obtained without ground truth except for the water level information. The water line determined from the reference scene which is the 2.7 m contour line is overlayed to the scene from which this depth map was retrieved in Figure 6. Comparison with the depth map (Figure 5) shows that it lies mainly between the 2 m and 3 m contours.

There is an area of negative depth (black area in Figure 5) which coincides with the area of apparently very shallow water, as can be judged from the behavior of the NIR values (see Figure 3 and 4). As can be seen from equation (4), the algorithm generates negative depths for values of the apparent reflectance that are above the zero depth value. Indeed, inspection of the image and of spatial profiles (Figure 3) shows that in the area in question, the apparent reflectance values at band 1 (green) and 2 (red) increase slightly, while NIR values decrease. This is likely to be caused by an increased amount of suspended matter in the water which causes backscattering to dominate over attenuation in shallow water; a discussion of this effect can be found in Ji et al. (1992).

The depth of deep areas (lower left in the map and the image) is apparently underestimated. A possible reason is that the attenuation coefficient in the deep water is smaller than near the shore because of lower turbidity and/or lower plankton concentration. This and the effect causing the negative depths mentioned above suggest that the assumption of a spatially homogenous attenuation coefficient (and other parameters) is probably too strong. This problem could be relaxed by splitting the area into smaller parts which are then analyzed separately. Another possible source of error is that the atmospheric conditions of the two scenes were too different. This causes differences in the path radiance (L_{PATH} in equation (1)) and thus in the radiance (and hence apparent reflectance $R(\infty)$). This would result in the first term on the right-hand side of equation (6) not being negligible.

Apart from that, there are a number of ways to improve the depth retrieval: (1) Include band 2 (red) in the calculations by using the band 1/band 2 band ratio instead of only band 1, as proposed in Philpot (1989). (2) Include all 3 bands

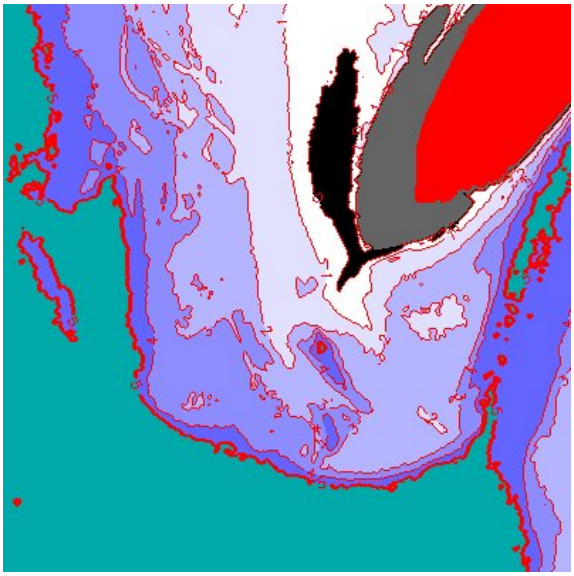

Figure 5: Depth retrieved from a scene acquired 22 January, 1998, 03:40:42 UTC, using a scene acquired on 27 March, 1998, 03:38:52 UTC as a reference. The color coding: Land Mud 0-1m, 1-2m , 2-3m , 3-4m 4-5m 5-10m 10-15m 15-20m negative depth

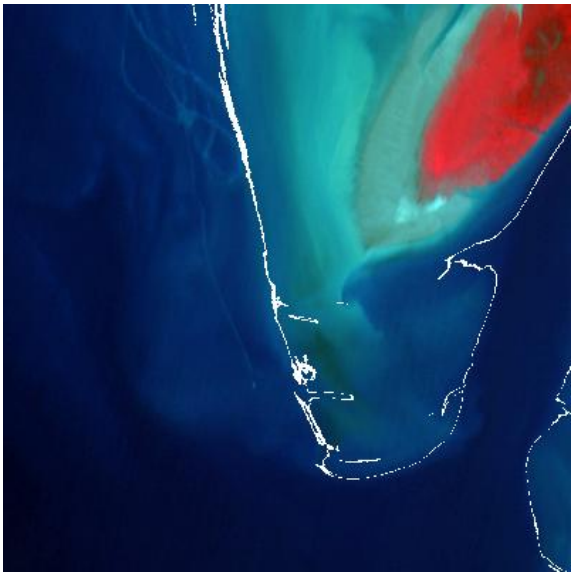

Figure 6: Image from which depth was retrieved (22 January, 1998, 03:40:42 UTC), with the pixels that are at the water line the reference scene in white. This should correspond to the 2.7 m depth contour. © CNES 1998

by using the "depth of penetration" (DOP) method proposed by Jupp (1988) (see also Green et al., 2000). The DOP method divides the image into zones according to the maximum penetration depth of the different bands and than deals with each zone separately, using estimated attenuation coefficients or locations with known water depth.

Another way to retrieve water depth information for just the intertidal area is to compile as many suitable scenes as possible, with different water levels, and determine the water line in each scene as described in section 4.1.

6. CONCLUSION

The present study shows ways to make use of multiple SPOT multispectral images of the same area in order to get information on the water depth. The water line can often be determined from the NIR data which then can be used to estimate the attenuation coefficient for individual scenes from ratios with reference scenes. There is room for some improvement and refinement.

APPENDIX

A.1 Effective Two-way Attenuation Coefficient

For the sun at a zenith angle ζ and a sensor with a viewing angle (off-nadir) θ, the path length in water of light reflected by the bottom is

$$\frac{z}{\cos\zeta'} + \frac{z}{\cos\theta'} \equiv f \cdot z \tag{7}$$

where z is the water depth, and ζ' and θ' are the solar zenith angle and the sensor's viewing angle in the water, respectively, as modified by the refraction at the water surface. Using the refractive index n of water and Snell's law in order to rewrite the above equation for the unmodified solar zenith angle ζ and sensor's viewing angle θ in the air, we get

$$f = \left[1 - \left(\frac{\sin\zeta}{n}\right)^2\right]^{-\frac{1}{2}} + \left[1 - \left(\frac{\sin\theta}{n}\right)^2\right]^{-\frac{1}{2}} \tag{8}$$

For the sensor used here (SPOT HRV), θ is less then 30°, and for the scenes investigated in this paper, the solar zenith angle at the time of image acquisition is always less than about 35°. Thus, the factor f is very close to 2 and at most 2.2. For larger zenith and viewing angles, f can become as large as 3.

REFERENCES

Benny, A.H., and G.J. Dawson, 1983. Satellite imagery as an aid to bathymetric charting in the Red Sea. The Cartographic Journal, 20 (1), pp. 5-16.

Green, E., A. Edwards, P. Mumby, 2000. Mapping Bathymetry. In: Remote Sensing Handbook for Tropical Coastal Management, by E.P. Green, P.J. Mumby, A.J. Edwards, C.D. Clark (edited by A.J. Edwards); Coastal Management Sourcebook 3, UNESCO Paris, pp. 219-233.

Hydrographic Branch, Royal Malaysian Navy, 1997, 1998, 2000. Tide Tables Malaysia, Volume 1.

Ji, W., D.L. Civco, W.C. Kennard, 1992. Satellite remote bathymetry: A new mechanism for modeling. Photogramm. Eng. and Remote Sens., 58 (5), pp.545-549.

Jupp, D.L.B., 1988. Background and extensions to depth of penetration (DOP) mapping in shallow coastal waters. Proceedings of the Symposium on Remote Sensing of the Coastal Zone, Gold Coast, Queensland, September 1988, pp. IV.2.1-IV.2.19.

Lyzenga, D.R., 1978. Passive remote sensing techniques for mapping water depth and bottom features. Applied Optics, 17 (3), pp. 379-383.

Melsheimer, C., L.K. Kwoh, 2001. Sun glitter in SPOT images and the visibility of oceanic phenomena. This issue (Proceed. 22nd Asian Conference on Remote Sensing, Singapore, Nov. 2001).

Mobley, C.M., 1994. Light and Water, Radiative Transfer in Natural Waters. Academic Press, Inc., San Diego, CA, 592 pp.

Philpot, W.D., 1989. Bathymetric mapping with passive multispectral imagery. Applied Optics, 28 (8), pp. 1569-1578.

Smith, R.C., and K.S. Baker, 1981. Optical properties of the clearest natural waters (200-800 nm). Applied Optics, 20 (2), pp. 177-184.